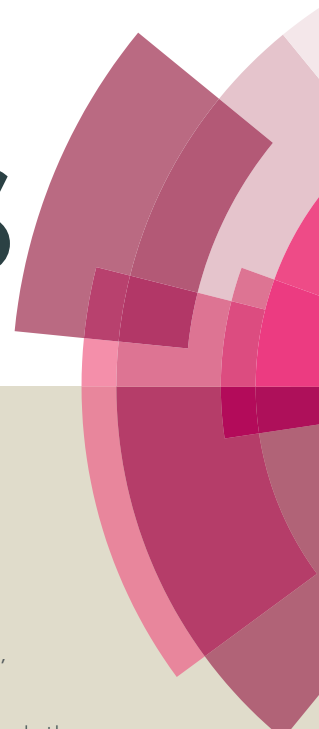


# RSC Advances



This article can be cited before page numbers have been issued, to do this please use: S. Jeon, H. Roh, D. J. Moon and J. W. Bae, *RSC Adv.*, 2016, DOI: 10.1039/C6RA09522D.



This is an *Accepted Manuscript*, which has been through the Royal Society of Chemistry peer review process and has been accepted for publication.

*Accepted Manuscripts* are published online shortly after acceptance, before technical editing, formatting and proof reading. Using this free service, authors can make their results available to the community, in citable form, before we publish the edited article. This *Accepted Manuscript* will be replaced by the edited, formatted and paginated article as soon as this is available.

You can find more information about *Accepted Manuscripts* in the [Information for Authors](#).

Please note that technical editing may introduce minor changes to the text and/or graphics, which may alter content. The journal's standard [Terms & Conditions](#) and the [Ethical guidelines](#) still apply. In no event shall the Royal Society of Chemistry be held responsible for any errors or omissions in this *Accepted Manuscript* or any consequences arising from the use of any information it contains.

Submitted to the *RSC Advances*

**Aqueous phase reforming and hydrodeoxygenation of ethylene glycol on  
Pt/SiO<sub>2</sub>-Al<sub>2</sub>O<sub>3</sub>: effects of surface acidity to product distribution**

**Seongho Jeon<sup>a</sup>, Hyun-Seog Roh<sup>b</sup>, Dong Ju Moon<sup>c</sup>, Jong Wook Bae<sup>a,\*</sup>**

<sup>a</sup>School of Chemical Engineering, Sungkyunkwan University (SKKU), Suwon, Gyeonggi-do,  
440-746, Republic of Korea

<sup>b</sup>Department of Environmental Engineering, Yonsei University, 1 Yonseidae-gil, Wonju,  
Gangwon-do, 220-710, Republic of Korea

<sup>c</sup>Clean Energy Research Center, Korea Institute of Science and Technology (KIST), 136-791  
Seoul, Republic of Korea

---

\*Corresponding author (J.W. Bae); Tel.: +82-31-290-7347; Fax: +82-31-290-7272; E-mail  
address: finejw@skku.edu

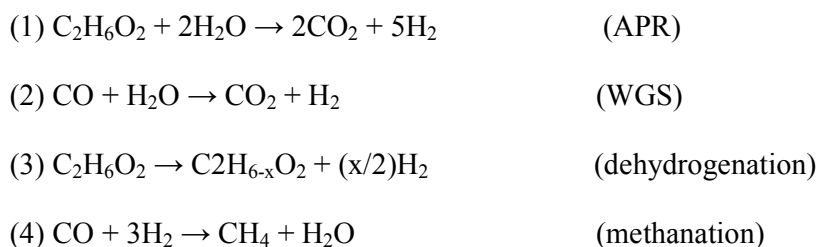
## ABSTRACT

Aqueous-phase reforming (APR) and aqueous-phase hydrodeoxygenation (APH) reaction of ethylene glycol (EG) were investigated using the platinum supported solid-acid  $\text{SiO}_2\text{-Al}_2\text{O}_3$  catalysts having different Si/Al molar ratios. The molar ratio of Si/Al on the  $\text{SiO}_2\text{-Al}_2\text{O}_3$  mixed metal oxides largely altered the surface area with its acidity as well as the reduction behavior of the supported platinum nanoparticles. The Pt/ $\text{SiO}_2\text{-Al}_2\text{O}_3$  catalysts having a Si/Al molar ratio of 0.1 showed a higher activity for APR as well as APH reaction. Among the various properties of Pt/ $\text{SiO}_2\text{-Al}_2\text{O}_3$ , the amount of acid sites on  $\text{SiO}_2\text{-Al}_2\text{O}_3$  supports largely changed EG conversion and production distribution with different coke depositions, and the acidic property was more dominant factor for catalytic activity than the platinum crystallite size with its reduction behavior. The easy and simultaneous cleavages of C-C as well as C-O bonds in EG on the Bronsted acid sites of Pt/ $\text{SiO}_2\text{-Al}_2\text{O}_3$  catalysts were responsible for a higher EG conversion and hydrocarbon formation. A larger amount of weak acid sites was also related with a larger hydrocarbon formation and a lower coke deposition. Compared with the Pt/ $\text{Al}_2\text{O}_3$ , the better catalytic acidity with a low coke deposition on the Pt/ $\text{SiO}_2\text{-Al}_2\text{O}_3$  at a Si/Al molar ratio of 0.1 was observed. It can be mainly attributed to the easy control of weak and strong acid sites with a high dispersion of platinum crystallites by simply changing a Si/Al molar ratio of the  $\text{SiO}_2\text{-Al}_2\text{O}_3$  mixed metal oxides.

**Keywords:** Aqueous-phase reforming (APR); Aqueous-phase hydrodeoxygenation (APH); Ethylene glycol (EG); Platinum;  $\text{SiO}_2\text{-Al}_2\text{O}_3$  mixed metal oxides; Surface acidity.

## 1. Introduction

Since the utilizations of traditional fossil fuels such as coal, crude oils and natural or shale gases can generate energy sources with an abundant emission of environmental pollutants, some renewable energy sources such as biomass-derived hydrogen can be one of alternative candidates to overcome environmental problems of fossil fuels having limited resources. For a complete carbon recycle, biomass-derived fuels have promising characters by some transformation processes such as gasification, pyrolysis, fermentation or chemical conversion processes and so on.<sup>1-3</sup> Among them, an aqueous-phase reforming (APR) reaction of biomass-derived intermediates seems to have many advantages due to its lower operating temperature and a high purity of hydrogen production with a lower concentration of CO. Generally, some supported novel metals such as Pt, Ru, Ir, Rh, Ni or Pd have been known to be active for the APR reaction with a higher selectivity to hydrogen.<sup>4</sup> Especially, Pt-supported catalysts on various supports such as Al<sub>2</sub>O<sub>3</sub>, SiO<sub>2</sub>, zeolites and Al<sub>2</sub>O<sub>3</sub>-SiO<sub>2</sub> and so on have been largely investigated for APR reaction through the characteristic reactions such as main APR reaction, water-gas shift (WGS) reaction, dehydrogenation, methanation and decomposition as represented in **Eq. 1** to **Eq. 4** using a biomass-derived model component of ethylene glycol (EG).<sup>5-7</sup>



The reaction pathways of APR reaction to generate hydrogen using EG feedstock have been generally known to proceed by first dehydrogenation reaction step of EG followed by the C-C cleavage and WGS reaction simultaneously. The methanation reaction is one of the main side reactions, which can be also strongly related with extents of coke formation.<sup>8,9</sup> Moreover,

the byproducts such as ethylene, CO and other oxygenates can also cause a severe coke formation on the catalysts surfaces as well.<sup>10-13</sup> The hydrogen and alkanes can be produced by separate C-C and C-O bond cleavages during APR reaction.<sup>14-17</sup> The oxygenates such as alcohols and acetaldehydes can be also formed by a simultaneous dehydration on Ru-based APR catalysts, however these oxygenated intermediates can be easily transformed to hydrogen and CO<sub>2</sub> by a facile WGS reaction as well.<sup>18</sup> The selective C-C or C-O bond cleavages have been generally known to generate various products during APR reaction, where C-C bond cleavage (**Eq. 5**) can selectively produce hydrogen and CO<sub>2</sub> with a combination of WGS reaction, and C-O bond cleavage (**Eq. 6**) can selectively produce hydrocarbons as well. The simultaneous C-O and C-C cleavages (**Eq. 7**) can also happen easily since these cleavages are very competitive reactions during APR reaction. The preferential activities of separate C-C or C-O bond cleavages are strongly depending on the types of active metals, which seems to be an important catalyst design factor due to a high O/C ratio of the biomass-derived intermediates.<sup>19</sup>



In addition, aqueous-phase hydrodeoxygenation (APH) reaction has been known as an efficient production method of alkanes and petrochemicals using biomass-derived chemicals with a similar catalytic system as explained for APR catalysts.<sup>20-22</sup> However, APH reaction requires a much higher activity for C-C cleavage to remove oxygen atoms by dehydration and to add hydrogen atoms through hydrogenation and hydrogenolysis as well. In general, the supported metal catalysts containing active palladium species have been known to be active for C=O and C=C bond cleavages in furfural by hydrogenation,<sup>23</sup> and those of ruthenium-based catalysts have been reported as the most active catalyst for APH reaction for an

activation of non-furanic carbonyl groups, which also requires different active sites compared to APR reaction. Therefore, APH catalysts generally require to possess different active sites for C-C cleavages through a retro-aldol condensation with decarbonylation on the metallic sites and C-O cleavages by selective dehydration on the acidic sites as well.<sup>24</sup> Based on the previous studies,<sup>15,22,25-30</sup> the C-C and C-O bond cleavages are competitive reactions at the very beginning of retro-aldol condensation and dehydration step on the metallic sites of the novel metals as well as on the acid sites of solid-acid surfaces.<sup>15,22,25,26</sup> In addition, the formed alcohols such as methanol during C-C and C-O bond cleavages can be converted to CO<sub>2</sub> and hydrogen by dehydrogenation followed by WGS reaction, which seems to be competitive reactions as well on the metallic platinum sites such as Pt(111) surfaces.<sup>27-30</sup> Among the competitive and complicated reactions during APR and APH reaction, the hydrogenation and dehydration steps have been known to be essential steps for an easy transformation of the biomass-derived intermediates. Those reactions selectively occur on heterogeneous or homogeneous catalytic systems by using bimetal or metal complexes with a combination of solid-acid zeolites and metal oxides as well.<sup>31-34</sup> In addition, hydrogenolysis and dehydration with a subsequent dehydrogenation reaction have been also largely investigated using some solid-acid catalysts to efficiently remove oxygen atoms in the biomass-derived reactants.<sup>35-40</sup>

In the present investigation, simple and prototype Pt/SiO<sub>2</sub>-Al<sub>2</sub>O<sub>3</sub> catalysts having different acidic properties due to different Si/Al ratios were investigated for APR and APH reactions to verify the roles of the amount and type of acidic sites for a different catalytic activity and product distribution. Even though some Pt-supported solid acid catalysts have been extensively reported, the comparative studies for APR and APH reaction using the same Pt/SiO<sub>2</sub>-Al<sub>2</sub>O<sub>3</sub> catalysts have been scarcely reported till now as far as we know, especially by comparing different hydrocarbon distribution according to the surface acidic properties.

## 2. Experimental section

### 2.1. Catalyst preparation and activity test of the Pt/SA catalysts

SiO<sub>2</sub>-Al<sub>2</sub>O<sub>3</sub> mixed metal oxides (SA) with a different Si/Al molar ratio from 0 to 1.0 were synthesized by coprecipitation method. For more detail, the SiO<sub>2</sub>-Al<sub>2</sub>O<sub>3</sub> solid acid supports were prepared using aluminum nitrate nonahydrate (Al(NO<sub>3</sub>)<sub>3</sub>•9H<sub>2</sub>O, Daejung) precursor and tetraethylorthosilicate (TEOS, Si(OC<sub>2</sub>H<sub>5</sub>)<sub>4</sub>, Alfa) precursor after dissolving separate precursors in a mixed solvent of deionized water and ethanol. The dissolved two separate metal precursors were vigorously stirred for 15 minutes separately, and the separate metal precursor solutions were mixed together carefully. For the subsequent coprecipitation of the above two solutions, 30vol% ammonia solution was dropped slowly into the mixed metal precursor solutions and it was stirred for 3 h at ambient temperature. As-prepared gel-like slurry was dried under a vacuum condition at 60 °C for 2 h and followed by drying at 110 °C overnight. Finally, the as-prepared sample was calcined at 300 °C for 4 h to prepare solid acid mixed metal oxide of SiO<sub>2</sub>-Al<sub>2</sub>O<sub>3</sub>.<sup>40</sup> For preparing platinum supported catalysts using the previously prepared SA supports, tetraammineplatinum (II) nitrate (Pt(NO<sub>3</sub>)<sub>4</sub>(NO<sub>3</sub>)<sub>2</sub>) precursor was loaded over the as-prepared SA support by incipient wetness impregnation method at a fixed platinum metal amount from 1 to 7wt% using a deionized water. The platinum supported SA catalysts were further dried overnight at 80 °C followed by calcining at 350 °C for 4 h. The as-prepared catalyst was denoted as Pt/SA(x), where SA stands for the solid-acid SiO<sub>2</sub>-Al<sub>2</sub>O<sub>3</sub> support and x for a different molar ratio of Si/Al. In addition, Pt(y)/SA(0.1) catalysts were also prepared similarly and y represent weight % of platinum metal on the SA(0.1) support.

APR reaction was carried out in a fixed-bed tubular reactor having an outer diameter of 9.5 mm at the reaction conditions of T = 250 °C, P = 4.5 MPa and weight hourly space velocity (WHSV) = 2.0 h<sup>-1</sup> for around 20 h using 0.3 g catalyst. Prior to activity test, the catalyst was reduced at 350 °C for 2 h under a flow of 5vol%H<sub>2</sub> balanced with N<sub>2</sub>. The reaction

temperature was adjusted using PID controller with K-type thermocouple, and the pressure was controlled by using back pressure regulator as well. The reactant of ethylene glycol (EG) with 10wt% in an aqueous solution (molar ratio of EG/H<sub>2</sub>O = 0.383) was fed to the reactor at a flow rate of 0.1 ml/min using HPLC pump (SP930D, YoungLin) with N<sub>2</sub> flow with a flow rate of 30 ml/min, which was used as a carrier and an internal standard gas. APH reaction was also carried out at a similar reduction and reaction condition with 0.5 g catalyst using a mixed gas of 80vol%H<sub>2</sub> balanced with N<sub>2</sub>. The catalytic activity was measured at the reaction conditions of T = 260 °C, P = 5.0 MPa and WHSV = 0.6 h<sup>-1</sup> for around 20 h. The effluent gases from the reactor were in-situ analyzed by using a gas chromatography (6500GC, YoungLin) equipped with thermal conductivity detector (TCD) connected with Carboxen 1000 column as well as flame ionization detector (FID) connected with HP-PLOT/Q capillary column. The conversion of EG and product distributions were calculated using the following equations based on an internal standard gas of N<sub>2</sub>, and the production rate of H<sub>2</sub> was also calculated using the produced moles of H<sub>2</sub> with a unit of mL/(g<sub>cat</sub> h).

- EG conversion to gaseous products (mol %) = (moles of C atoms in a gas-phase / moles of C atoms in the EG feed) \*100
- Selectivity of gaseous products (mol %) = (moles of selected product in a gas-phase / total moles of carbons formed in a gas-phase) \*100

## 2.2. Catalyst characterizations

Powder X-ray diffraction (XRD) patterns of the fresh and used Pt/SA catalysts were obtained using D8 ADVANCE (Bruker) instrument with a Cu-K $\alpha$  radiation of wavelength of 15.406 nm at an operating voltage of 40 kV with a scanning rate of 4°/min in the diffraction range of 2 $\theta$  = 20 - 70° to verify the crystalline phases and crystallite sizes. The crystallite sizes of the supported platinum nanoparticles were calculated using a value of full width at

half maximum (FWHM) by using Debye-Scherrer equation with the most intensive diffraction peak of metallic platinum at  $2\theta = 40.0^\circ$ . Thermogravimetric analysis (TGA) of the used Pt/SA catalysts was carried out by using Seiko Exstar 6000 (TG/DTA6100) to confirm the quantity of the deposited cokes after APR reaction for 20 h on stream. The Si/Al molar ratio of the mixed metal oxides was further characterized by X-ray fluorescence (XRF) analysis using Bruker AXS S4 Pioneer that operated at 60 kV and 150 mA.

Specific surface area, pore volume and average pore diameter were measured by  $N_2$  adsorption-desorption analyses using Micromeritics TriStar II instrument working at liquid nitrogen temperature of  $-196^\circ\text{C}$ . The specific surface area of the fresh Pt/SA catalysts was calculated by Brunauer-Emmett-Teller (BET) method, and average pore diameter and its pore size distribution were measured by Barrett-Joyner-Halenda (BJH) method from the desorption isotherm. Prior to analysis, the sample was pretreated by degassing at 90 and  $350^\circ\text{C}$  for 4 h consecutively. In addition,  $H_2$  chemisorption analysis of the Pt/SA catalysts was also carried out by using Micromeritics ASAP 2020 instrument. The metal surface area and dispersion of the supported platinum nanoparticles were obtained by using adsorbed amount of hydrogen at  $35^\circ\text{C}$  on the reduced Pt/SA catalyst. Prior to analysis, the sample was pretreated under vacuum condition of 10 mmHg at  $300^\circ\text{C}$  for 2 h to remove any impurities on the Pt/SA surfaces. The sample was subsequently reduced at  $350^\circ\text{C}$  for 2 h, which is the same condition of the reduction step before APR reaction. The dispersion, metal surface area and crystallite size of the supported platinum nanoparticles were calculated with an assumption of a stoichiometry number (H/Pt) of 1.0.

Temperature-programed reduction with  $H_2$  (TPR) and temperature-programed desorption of ammonia ( $NH_3$ -TPD) were separately measured by using Belcat-M (Bel Japan) instrument equipped with TCD. Prior to TPR analysis, 30 mg of the fresh Pt/SA catalyst was pretreated at  $250^\circ\text{C}$  under a flow of argon to remove any impurities and water adsorbed on the surfaces.

TPR patterns were obtained with a ramping rate of 10 °C/min under a flow of 10vol% H<sub>2</sub> balanced with argon. The formed water from the TPR experiment was selectively removed by using molecular sieve trap, and the hydrogen consumption was measured by TCD. For the analysis of NH<sub>3</sub>-TPD, 30 mg of the fresh Pt/SA catalyst was loaded in a quartz tube reactor and the sample was pretreated at 250 °C for 2 h under a flow of He. After that, ammonia gas was adsorbed at 50°C for 30 minutes and the physisorbed ammonia was removed by flushing it under He flow at the same temperature for 1 h. Finally, the amount of the desorbed ammonia was measured by TCD under He flow in the temperature range of 100 - 600 °C at a ramping rate of 10 °C/min. The surface morphologies and the variation of crystallite sizes on the fresh and used fresh Pt/SA(0) and fresh Pt/SA(0.1) after APR reaction were characterized using transmission electron microscopy (TEM) with a TECNAI G2 instrument operated at an accelerating voltage of 200 kV.

Fourier transformed infrared (FT-IR) spectroscopy of the adsorbed pyridine (Py-IR) was applied to characterize the types of acid sites such as Bronsted and Lewis sites on the fresh Pt/SA catalysts. Using in-situ IR cell equipped with CaF<sub>2</sub> window and shelf-supported thin pellet of the Pt/SA catalyst which was previously mixed and pelletized with an excess KBr powder with a mass ratio of 100:1, the Py-IR experiment was carried out. For a selective adsorption of pyridine probe molecules on the acid sites, the pyridine were previously flowed on to the pellet using N<sub>2</sub> gas carrier at room temperature for 30 min. After the physisorbed pyridine was selectively evacuated for 45 min under vacuum condition, the chemically adsorbed pyridine absorption band spectra were obtained after subtracting background peaks obtained before an adsorption of pyridine on the fresh Pt/SA catalyst.

### 3. Results and discussion

#### 3.1. Catalytic activities of the APR and APH reaction

The catalytic activities for APR reaction of EG on the Pt/SA catalysts at a fixed platinum metal content of 5wt% are summarized in **Table 1** in terms of conversion of EG to gaseous products and product distributions, where SA(x) represents the solid-acid SiO<sub>2</sub>-Al<sub>2</sub>O<sub>3</sub> for SA with x digit for a molar ratio of Si/Al, and SA(0) for the Al<sub>2</sub>O<sub>3</sub> support. The EG conversions to gaseous products were maximized on the Pt/SA(0.1) with 43.4% and a maximum H<sub>2</sub> production rate of 1691 mL/(g<sub>cat</sub> h), which were the averaged values at a steady-state after the reaction of 15 h on stream. A typical volcano pattern of EG conversions and product distributions was observed on the Pt/SA catalysts. The lowest EG conversion was observed on the Pt/SA(1.0) with the value of 18.4%, which seems to be responsible for an observed high CO selectivity of 5.2% with a lower CO<sub>2</sub> selectivity due to a suppressed WGS activity of the intermediates derived from C-C bond cleavages of EG. Interestingly, the hydrocarbon selectivity was decreased with an increase of Si/Al molar ratios of the Pt/SA catalysts from 0.9% on the Pt/SA(0.1) to 2.5% on the Pt/SA(1.0), except for the Pt/SA(0). This observation seems to be attributed to a higher dehydrogenation activity for the C-C bond cleavages on the catalysts having a larger amount of Bronsted acid sites.<sup>8,9</sup> Most interesting observation is a significantly different hydrocarbon distributions by showing an increasing trend of CH<sub>4</sub> selectivity from 20.5 to 64.5% and vice versa in that of C<sub>2</sub>H<sub>6</sub> from 79.5 to 35.3% with an increase of Si/Al ratios. This observation can be attributed to a different acidity of the SiO<sub>2</sub>-Al<sub>2</sub>O<sub>3</sub> surfaces by largely changing the intrinsic activities of C-C and C-O bond cleavages. Based on these observations, a higher conversion of EG to gaseous products is responsible for a higher H<sub>2</sub> production rate with a lower selectivity of CO and hydrocarbons with the help of the enhanced WGS activity, except for the Pt/SA(0). Even though the Pt/SA(0) showed a lower conversion of EG around 27.5%, a higher selectivity to H<sub>2</sub> and a lower selectivity to CO were observed due to a possible coke deposition on the too strong acidic sites with a higher WGS activity on the largely exposed platinum metal surfaces. Compared to other

Pt/SA catalysts which showed a stable EG conversion to gaseous products even after 15 h on stream, a significant decrease of EG conversion on the Pt/SA(0) during 15 h on stream can be possibly attributed to a severe coke deposition as shown in **Figure 1**. The steady increases of the EG conversion to gaseous products for 15 h on stream can be due to a possible surface rearrangement of the supported platinum crystallites and an easy phase transformation of alumina species. It can be also attributed to a hydrogen gas residue used for reduction step of Pt/SA catalysts and for a pressure adjustment step at 5.0 MPa before APR reaction. However, the comparisons of the catalytic activities at steady-state after 15 h on stream seem to be reasonable since the similar catalytic activity changes according to a Si/Al ratio on the Pt/SA catalysts were observed at similar EG conversions as summarized in supplementary **Table S1**. The selectivity to hydrocarbons on the Pt/SA catalysts seems to be mainly caused by a presence of the acidic sites having a proper acid strength, which seems to be increased with an increase of the surface acid sites.<sup>35-39</sup> The selectivity of hydrocarbons such as C<sub>1</sub> and C<sub>2</sub> paraffinic species seems to increase on the weak acid sites of SiO<sub>2</sub>-Al<sub>2</sub>O<sub>3</sub> preferentially by a possible decomposition of the intermediates derived from EG, which can be dehydration or retro-aldol condensation reactions. To verify the effects of acid sites during the consecutive reactions of EG conversion, the most active Pt/SA(0.1) catalyst was further examined at different space velocities such as 1.0 and 0.5 h<sup>-1</sup> and the results are summarized in **Table 1**. The conversions of EG to gaseous products at different space velocities are displayed in supplementary **Figure S1**. With a decrease of space velocities from 2.0 to 0.5 h<sup>-1</sup> on the Pt/SA(0.1) at T = 250 °C and P = 4.5 MPa, the conversion of EG steadily increased from 43.4 to 78.6% without the significant changes of product distributions except for the hydrocarbons from 0.9 to 2.0% with a significant variation of C<sub>1</sub> from 36.2 to 78.1 % and C<sub>2</sub> from 63.8 to 21.9%. These results strongly suggest that the intermediates such as aldehydes and alcohols formed from the APR reaction of EG can be further reacted to form hydrocarbons, especially

for CH<sub>4</sub> hydrocarbon at a longer residence time. It also revealed that the Bronsted acidic sites having weak acid strengths and small metallic platinum crystallites (confirmed by NH<sub>3</sub>-TPD and TPR in next section) are responsible for further transformation of the intermediates to light hydrocarbons, which seems to be similar effects of longer residence times of the intermediates formed by simultaneous C-O and C-C bond cleavages of EG reactant. Interestingly, the hydrocarbon formation rate on the Pt/SA catalysts having a higher Si/Al ratio above 0.4 was stabilized after 10 h on stream as shown in supplementary **Figure S2**, which can be possibly attributed to the presence of a relatively larger amount of Bronsted acid sites. As summarized in supplementary **Table S2**, a higher hydrocarbon formation was observed on the large amount of Pt-containing Pt(7)/SA(0.1) catalyst with the value of 5.0% with CH<sub>4</sub> selectivity of 88.6%. The large amount of the metallic platinum content seems to be responsible for the further reactions of intermediates to hydrocarbons. However, conversion of EG to gaseous products was not significantly increased on the Pt/SA(0.1) having a large amount of platinum above 3wt% except for the Pt(1)/SA(0.1) due to an easy aggregation of the supported platinum crystallites at a high platinum content on the SA(0.1) support with facile phase transformations of alumina.

To further verify the roles of the acidity of SA supports according to Si/Al ratios to the hydrocarbon selectivity and EG conversion, APH reaction was further carried out on all Pt/SA catalysts and the results are summarized in **Table 1**. The variations of EG conversion to gaseous products were found to be similar with those of APR reaction with the highest conversion of 47.9% on the Pt/SA(0.1) and lowest on the Pt/SA(1.0) with 29.0% at steady-state. CO<sub>2</sub> selectivity was decreased with an increase of Si/Al ratio from 96.2% on the Pt/SA(0) to 76.3% on the Pt/SA(1.0) due to a lower WGS activity of the intermediated formed from the C-C bond cleavage by the dehydration of EG possibly. However, CO selectivity was varied inversely by increasing from 1.1% on the Pt/SA(0) to 14.7% on the

Pt/SA(1.0) with an increase of Si/Al ratio of the Pt/SA catalysts. This observation suggests that the catalytic activities of APR and WGS reaction are strongly influenced by the amount of active metal surface area as well as the acid sites during the aqueous-phase reaction. At a higher partial H<sub>2</sub> pressure during APH reaction, hydrogenation activity can be increased by enhancing the C-C bond cleavage of EG due to the additionally formed H<sub>2</sub> by WGS reaction. Therefore, the increased hydrocarbon selectivity from 2.7 to 9.0% and its production rate from 1.4 to 3.1 mL/(g<sub>cat</sub>·h) with an increase of Si/Al molar ratio during APH reaction can support an enhanced hydrogenation activity, which was significantly increased with an increase of Si/Al ratio on the Pt/SA catalysts. As shown in **Figure 2**, the catalytic activity for APH reaction with time on stream seems to be more stable than APR reaction without showing a significant deactivation after 10 h on stream. Interestingly, the variations of C<sub>1</sub> – C<sub>3</sub> paraffinic hydrocarbon selectivity for APH reaction were found to be similar with those of APR reaction with same trends by showing a higher selectivity of hydrocarbons on the Pt/SA catalyst having larger Bronsted acid sites. The increase of C<sub>1</sub> selectivity from 46.0 to 56.1% and decrease of C<sub>2</sub> selectivity from 50.9 to 42.8% were observed with an increase of Si/Al ratio on the Pt/SA catalysts, which suggests that the different acidity of the SiO<sub>2</sub>-Al<sub>2</sub>O<sub>3</sub> surfaces and metallic surface area of platinum crystallites can largely alter the C-C and C-O bond cleavages as well. The production rates of the hydrocarbons on the Pt/SA catalysts are displayed in the supplementary **Figure S3**. At a high Si/Al ratio above 0.4, the significant stability of the hydrocarbon formation rate with time on stream seems to be attributed to a lower coke deposition with a large amount of Bronsted acid sites as well. From the observed catalytic activities for APR as well as APH reaction on the Pt/SA catalysts having a different Pt loading and space velocity, an optimal Pt/SA(0.1) was found to be proper to obtain a higher conversion of EG and hydrogen production rate. The product distribution was significantly affected by the surface properties such as a density and type of acid sites with a

surface area of the active platinum metal nanoparticles, which can also change hydrocarbon distributions through C-C and C-O bond cleavages of intermediates formed from EG reactant.

### 3.2. Physicochemical surface properties of the Pt/SA catalysts

The physicochemical properties such as specific surface areas, pore volumes and average pore diameters of the Pt/SA catalysts and SA supports measured by N<sub>2</sub> adsorption-desorption methods are summarized in **Table 2**. The Pt/SA catalysts prepared by coprecipitation method of the SA supports and a subsequent impregnation of platinum metal precursor showed surface areas above 300 m<sup>2</sup>/g by increasing from 302 m<sup>2</sup>/g on the Pt/SA(0) to 384 m<sup>2</sup>/g on the Pt/SA(1.0) with an increase of Si/Al molar ratio. An actual molar Si/Al ratio on the SA supports was found to be 0.12, 0.46 and 0.89 on the SA(0.1), SA(0.4) and SA(1.0), respectively, which were measured by XRF analysis. From the observed variations of surface areas of the SA supports from 370 to 496 m<sup>2</sup>/g, the decreased surface area of the Pt/SA catalysts was attributed to a partial pore blockage of the pore mouths through platinum metal deposition. These aggregation phenomena are the well-known segregation process by a deposition of the impregnated metal nanoparticles on the outer mesopores, which can be induced during a drying or calcination step.<sup>18,41</sup> The pore volumes of the Pt/SA catalysts were increased with an increase of surface area in the range of 0.24 – 0.55 cm<sup>3</sup>/g, and the average pore diameter was found to be larger on the Pt/SA catalysts with the size of 4.6 – 5.2 nm than that of the Pt/AS(0) due to possible intra-particle pore formation on the SiO<sub>2</sub>-Al<sub>2</sub>O<sub>3</sub> support. A pore size distribution on all the Pt/SA catalysts showed a unimodal pore size distributions as shown in supplementary **Figure S4**. Since the specific surface area and average pore diameter were not significantly altered on all fresh Pt/SA catalysts, these physical properties seem to insignificantly change the catalytic activity of APR<sup>41</sup> and APH reaction as well.

Therefore, the dispersion, surface area and crystallite size of the supported metallic platinum on the fresh Pt/SA catalysts were further measured by H<sub>2</sub> chemisorption, and the results are summarized in **Table 2**. The dispersions of metallic platinum crystallites were found to be in the range of 45.7 – 63.9%, where it was lower on the Pt/SA(0) with the value of 45.7% than other Pt/SA catalysts having the value of above 60%. In addition, a larger crystallite size of 2.54 nm and smaller surface area of metallic platinum of 5.64 m<sup>2</sup>/g<sub>Pt</sub> were also observed on the Pt/SA(0), however the values were found to be similar on the other Pt/SA catalysts in the ranges of 1.81 – 1.86 nm and 7.65 – 7.89 m<sup>2</sup>/g<sub>Pt</sub>, respectively. Generally, a larger crystallite size and smaller surface area of metallic platinum crystallites are known to be responsible for a lower hydrogenolysis and WGS activity.<sup>18,41</sup> The variations of platinum crystallite sizes can significantly alter an activity as well as a deactivation rate, and some active metal particles are preferentially sintered during the reaction, which resulted in altering the catalytic stability as well.<sup>42-48</sup> Therefore, the observed high selectivity of CH<sub>4</sub> on the Pt/SA(0.4) and Pt/SA(1.0) compared with the Pt/SA(0) can be attributed to a higher surface area of metallic platinum crystallites by the possible methanation activity after C-C and C-O bond cleavages of the intermediates.<sup>5-9,14-17</sup> However, since there was no direct correlation of EG conversion with the surface area of metallic platinum crystallites, we believe that the observed different catalytic activity and product distribution seem be originated preferentially from the other surface properties of the Pt/SA catalysts such as the density and type of acid site, aggregation of active metals and coke deposition and so on.

The crystalline structures and phases of the Pt/SA catalysts measured by XRD analyses are displayed in **Figure 3** and the supplementary **Figure S5** on the used and fresh Pt/SA catalysts, respectively. Some crystalline phases of platinum crystallites and boehmite-phase alumina ( $\gamma$ -AlOOH) were clearly observed on the fresh Pt/SA(0), however, only platinum crystallite phases were observed on the other fresh Pt/SA(0) and Pt/SA(0.1) due to the presence of the

amorphous phases of the  $\text{SiO}_2\text{-Al}_2\text{O}_3$  mixed metal oxides with highly dispersed platinum crystallites.<sup>42,49</sup> A larger characteristic peak intensity of platinum crystallites was observed on the fresh Pt/SA(0) and Pt/SA(0.1), which strongly suggests larger platinum crystallite formation compared with other Pt/SA catalysts, and these results were also supported by  $\text{H}_2$ -chemisorption and TEM analysis. Interestingly, the fresh Pt/SA(0) showed a characteristic  $\gamma\text{-AlOOH}$  and Pt(111) phases at the diffraction peak positions of  $2\theta = 40.0, 47.5$  and  $68.0$ , which revealed a phase transformation of  $\gamma$ -alumina to boehmite phase resulted in strongly interacting with a supported platinum nanoparticles.<sup>42</sup> As shown in **Figure 3**, the aggregation of platinum crystallites after APR reaction measured by XRD analysis was significant on the used Pt/SA catalysts with an average platinum crystallite size of 5.8, 2.2, 2.5, and 2.8 nm on the Pt/SA(0), Pt/SA(0.1), Pt/SA(0.4) and Pt/SA(1.0), respectively. In addition, the extent of transformation to  $\gamma\text{-AlOOH}$  phases was much significant on the Pt/SA(0) after APR reaction, and a significant coke deposition was observed only on the Pt/SA(0) by showing the characteristic peak of coke precursor at around  $2\theta = 23^\circ$ . The larger aggregation phenomena of platinum crystallites on the Pt/SA(0) with a large extent seems to be mainly attributed to a smaller amount of surface acidic sites and its easy transformation to the boehmite phases through a weak interaction of platinum crystallites compared with other Pt/SA catalysts. In addition, the observed larger amount of coke deposition on the Pt/SA(0) can be also originated from the presence of the strong acid sites on the  $\text{Al}_2\text{O}_3$  or boehmite phases, which can largely altered EG conversion and product distribution during APR and APH reaction as well.<sup>25-30</sup> The extent of coke deposition on the used Pt/SA catalysts after APR reaction for the duration of 20 h was further characterized by thermogravimetric analysis (TGA). In general, a weight loss (%) measured in a temperature range of 300 - 600 °C can be attributed to an oxidation of the deposited graphitic carbons.<sup>49</sup> As shown in **Table 2** and supplementary **Figure S6**, a significant coke deposition with the amount of 10.0wt% was observed on the

Pt/SA(0). A relatively smaller amounts of coke deposition in the range of 3.9 - 5.5wt% were observed on the other Pt/SA catalysts with the lowest value of 3.9wt% on the Pt/SA(0.1), which was the most active catalyst for APR and APH reaction. The inactive coke precursors can be generally formed over strong acidic sites from unstable intermediates during APR reaction.<sup>12</sup> However, a facile hydrogen spillover characters on the surfaces can suppress coke formations by hydrogenolysis reaction.<sup>50</sup> The ratio of Bronsted/Lewis acid sites can also significantly alter the adsorption characters of oxygenates formed, which can also promote coke depositions with a severe deactivation, especially on the strong Bronsted acidic sites.<sup>10,51</sup>

A reducibility of platinum crystallites on the Pt/SA catalysts was further verified by TPR experiments and the reduction behaviors of those catalysts are displayed in **Figure 4**, and the consumed amount of hydrogen are summarized in **Table 2**. The broad reduction peaks on the Pt/SA catalysts were observed at a maximum temperature at around 350 °C with a shoulder peak at around 430 °C, which suggests a relatively homogeneous distribution of platinum nanoparticles, except for the Pt/SA(0). However, multiple reduction peaks were observed on the Pt/SA(0) which suggests the distribution of the various platinum crystallite sizes on the Al<sub>2</sub>O<sub>3</sub> support. A lower reduction temperature peak at around 180 °C on the Pt/SA(0) seems to be responsible for a decomposition of platinum metal precursor with an easy reduction character (assigned to T<sub>L</sub>). In addition, a medium reduction temperature peak at around 350 °C (assigned to T<sub>M</sub>) on the Pt/SA catalysts can be assigned to the reduction of well-dispersed platinum nanoparticles on the SA surfaces. The reduction behaviors of supported platinum crystallites are strongly affected by the surface properties of silica-alumina mixed oxides by changing the platinum-support interactions.<sup>42,52</sup> Therefore, a higher temperature reduction peak (assigned to T<sub>H</sub>) can be responsible for the strongly interacted platinum nanoparticles only on the Al<sub>2</sub>O<sub>3</sub> support.<sup>41,53</sup> Interestingly, the amount of hydrogen consumption assigned to T<sub>M</sub> peak was increased with an increase of Si/Al ratio from 87 to 188 μmol/g<sub>cat</sub> without a

significant variation of the amount of  $T_L$  peak except for the Pt/SA(0). It seems to be attributed to the enhanced acidic sites of the bare SA supports by forming strongly interacted and well-dispersed platinum nanoparticles on strong acidic  $\text{SiO}_2\text{-Al}_2\text{O}_3$  supports.<sup>42,52</sup> These characteristic reduction behaviors of the supported platinum nanoparticles also significantly alter the WGS activity and C-C and C-O bond cleavages<sup>20-23,27-30</sup> by hydrogenation and hydrogenolysis reaction of intermediates formed by EG conversion, especially by altering the hydrocarbon selectivity.

To further verify effects of acid sites to platinum metal dispersion and reduction behavior on the solid acid SA supports,  $\text{NH}_3$ -TPD analysis was carried out on the fresh Pt/SA catalysts and the desorption patterns are displayed in **Figure 5** and the amount of desorbed  $\text{NH}_3$  are summarized in **Table 2**. The desorption peaks of  $\text{NH}_3$  showed two characteristic peaks at a maximum desorption temperature of around 200 °C (assigned to  $T_w$  for a desorbed amount of  $\text{NH}_3$  below 300 °C) and 450 °C (assigned to  $T_s$  for that between 300 – 500 °C), which can be also assigned to weak and strong acidic sites, respectively.<sup>54-56</sup> With an increase of Si/Al molar ratio on the Pt/SA catalysts, the desorbed amount of  $\text{NH}_3$  from weak acidic sites ( $T_w$ ) was increased and that of strong acidic sites ( $T_s$ ) and total acidic sites ( $T_{\text{tot}}$ ) were decreased steadily. In general, the Si-OH and  $\text{Al}^{3+}$  ions on the mixed metal oxides are known to be responsible for Brønsted (B) and Lewis acidic sites (L), respectively.<sup>35-40,54-56</sup> As summarized in **Table 2**, weak acid sites was increased and finally approach a constant value from 0.45 mmol/g<sub>cat</sub> on the Pt/SA(0) to 0.75 mmol/g<sub>cat</sub> on the Pt/SA(1.0). However, the amount of strong acid sites was decreased from 5.94 mmol/g<sub>cat</sub> on the Pt/SA(0) to 3.80 mmol/g<sub>cat</sub> on the Pt/SA(1.0) as similar for total acid sites ( $T_{\text{tot}}$ ) with an increase of Si/Al ratio on the Pt/SA catalysts. Therefore, the changes of the molar ratio of Si/Al on the mixed  $\text{SiO}_2\text{-Al}_2\text{O}_3$  metal oxides largely altered the surface acidic properties with various concentrations of Brønsted and Lewis acid sites. As measured by  $\text{NH}_3$ -TPD for total amount and strength of acid sites on

the Pt/SA catalysts, the types of the acid sites such as Brønsted and Lewis acid sites were further characterized by fourier-transformed infrared analysis of adsorbed pyridine molecules (Py-IR). To further verify the B/L ratio on the Pt/SA catalysts, the characteristic absorption bands of pyridine molecules assigned to Bronsted acid sites (B) at a wavenumber of  $1550\text{ cm}^{-1}$ , Lewis acid sites (L) at  $1450\text{ cm}^{-1}$ , and combined Bronsted and Lewis acid sites (B+L)<sup>54,55</sup> at  $1480\text{ cm}^{-1}$  were integrated and compared of the each pyridine peak. The B/L ratio on the Pt/SA catalysts as summarized in **Table 2** was increased with an increase of Si/Al ratio by showing the ratio of from 0 to 1.22. This observation strongly suggests that the amounts of Bronsted acid sites are increased with the increase of Si/Al molar ratio on the Pt/SA catalysts. These different amounts and types of the acid sites on the Pt/SA catalysts can largely alter the dispersion of platinum nanoparticles. This variation also change product distribution and EG conversion to gaseous products during APR and APH reaction by significantly altering the activities of C-C and C-O bond cleavages.<sup>20-23,27-30</sup>

### 3.3. Roles of acidic sites and metal surface area for hydrocarbon distribution

APR and APH reaction of the biomass-derived intermediates have been generally known to proceed through complicated reaction pathways such as dehydrogenation, the C-C and C-O cleavages and WGS reaction on the active metals and acid sites as well.<sup>10,14,43,57</sup> Therefore, a higher CO<sub>2</sub> selectivity and H<sub>2</sub> production rate can be obtained using hybrid catalysts having highly dispersed active metallic sites on the solid-acid sites of some mixed metal oxides. In addition, the solid-acid catalysts after properly modifying Bronsted and Lewis acid sites can also largely promote a dehydration activity of the biomass-derived intermediates.<sup>17,25,38,58</sup> From our previous work,<sup>41</sup> conversion of EG to gaseous products for the APR reaction was mainly depending on the dispersion of platinum crystallites on the mixed metal oxides of CeO<sub>2</sub>-ZrO<sub>2</sub> and a highly dispersed and larger surface area of metallic platinum crystallites on

ceria-zirconia support showed a higher EG conversion and hydrogen productivity.<sup>41</sup> However, the catalytic activity on the solid-acid hybrid Pt/SA catalysts showed somewhat different catalytic behaviors by showing the significant effects of the acidic sites on the solid-acid SiO<sub>2</sub>-Al<sub>2</sub>O<sub>3</sub>, which also modified the interactions of platinum nanoparticles with the acidic sites on the solid-acid SiO<sub>2</sub>-Al<sub>2</sub>O<sub>3</sub> support as well.

The observed higher selectivity to CO<sub>2</sub> and H<sub>2</sub> with a higher EG conversion to gaseous products on the Pt/SA(0.1) with a lower alkane formation with the values of 43.3% for APR reaction and 47.9% for APH reaction were mainly attributed to the highly dispersed platinum nanoparticles with the abundant presence of total acidic sites as summarized in **Table 1** and **Table 2**. However, the observed lower activity on the Pt/SA(0) was mainly attributed to the significant coke deposition due to the abundant strong acid sites for strong adsorption of intermediates. The lower alkane selectivity for APR reaction on the Pt/SA(0.1) seems to be also attributed to a higher activity for the C-O and C-C cleavages on the metallic platinum crystallites as well as on the acidic sites of the SiO<sub>2</sub>-Al<sub>2</sub>O<sub>3</sub> surfaces. Interestingly, the hydrocarbon selectivity especially for CH<sub>4</sub> was increased with an increase of Si/Al ratio and vice versa for C<sub>2</sub> hydrocarbons. Therefore, to further verify the effects of acid sites for the hydrocarbon selectivity, supplementary APH reaction was also carried out. The variations of EG conversion and product distribution were similar with the results of APR reaction except for the higher hydrocarbon productivity. Hydrocarbon selectivity was well correlated with the amount of weak Bronsted acid sites, and EG conversion was correlated with the amount of strong acid sites, which seem to be reasonable by the selective C-C and C-O cleavages on the strong acidic sites followed by hydrogenation and WGS activity on the platinum metallic sites as well as weak acidic sites, except for the Pt/SA(0) due to a fast deactivation by a severe coke deposition as confirmed by NH<sub>3</sub>-TPD, Py-IR, and TGA analyses. In addition, the observed higher CO<sub>2</sub> and H<sub>2</sub> selectivity on the Pt/SA(0.1) during APR and APH reaction

seem to be attributed to highly dispersed platinum nanoparticles with a proper interaction with  $\text{SiO}_2\text{-Al}_2\text{O}_3$  surfaces as confirmed by TPR and  $\text{H}_2$  chemisorption. We believe that an increased selectivity of  $\text{CH}_4$  on the Pt/SA(0.1) can be possibly attributed to a highly dispersed platinum nanoparticles as well as the abundant weak Bronsted acid sites due to the enhanced WGS activity on the active metallic sites. The TEM images on the selected Pt/SA catalysts before and after APR reaction are displayed in **Figure 6**, and a less aggregation of the well-dispersed platinum nanoparticles with a size of below 5 nm was observed on the Pt/SA(0.1) (**Figure 6(B-1)** and **(B-2)**). This revealed a less aggregation of platinum crystallites on the Pt/SA(0.1) compared with the Pt/SA(0) with a significant aggregation of platinum crystallites between 5 – 10 nm (**Figure 6(A-1)** and **(A-2)**), which was well matched with the results of XRD analysis as well. In general, the acid site density plays an important role to enhance a heat of adsorption and interaction between the biomass-derived intermediates on the acid sites, which can largely change the product distribution and conversion of the biomass-derived chemicals.<sup>59-61</sup> These phenomena were also confirmed by changing the residence time of reactants and platinum metal loading as shown in **Table 1** and the supplementary **Table S2**, and a longer residence time and a high loading of platinum metals are responsible for a high formation rate of  $\text{CH}_4$  as well as  $\text{H}_2$  and  $\text{CO}_2$  through an enhanced hydrogenolysis and WGS activity. These activity changes can be also attributed to a further dehydration of the intermediates formed through dehydration and hydrogenation of EG reactant. Therefore, the hydrocarbon formation during APR reaction seems to follow consecutive reaction pathways through dehydrogenation over metallic platinum nanoparticles followed by hydrogenolysis of the dehydrogenated intermediates through C-C and C-O cleavage mainly on the acid sites and further WGS reaction on the platinum metallic sites as well. Since  $\text{C}_2$  hydrocarbon can be formed by the selective C-C and C-O cleavage followed by hydrogenation on the metallic sites,  $\text{C}_2$  selectivity was decreased with an increase of Si/Al

molar ratio due to a decreased amount of the strong acid sites on the Pt/SA catalysts having a larger Si/Al molar ratio.

According to the previous study for APR reaction combined with Fischer-Tropsch synthesis reaction in a batch reacting system,<sup>62</sup> the acid component such as sulfuric acid strongly influences CO production rate and subsequently changes the activity of Fischer-Tropsch synthesis. The conversion of biomass-derived reactants to gaseous products has been known to be influenced by an initial step activity of dehydrogenation and dehydration, and the dehydrogenated intermediates can further proceed by dehydrogenation reaction to form hydrocarbons.<sup>57,58,63</sup> In addition, the solid-acid metal oxides after a modification of Bronsted and Lewis acid sites can largely change the dehydration activity as reported previously by many researches.<sup>38,64</sup> It has been well known that an increase of Si contents on the solid-acid Al<sub>2</sub>O<sub>3</sub>-SiO<sub>2</sub> catalysts can increase B/L ratio by producing an active Si-OH species on the surfaces.<sup>65</sup> In addition, a decrease of surface acidity can be attributed to a lower metal-oxygen bond energy in the order of Al-O > Zr-O > Si-O, which seems to be related with a large formation of oxygen vacant sites in the mixed metal oxides, which is assigned to Lewis acid sites.<sup>66,67</sup> Therefore, a higher Si/Al ratio on the present Pt/SA catalysts was responsible for a higher ratio of B/L which also changes hydrocarbon distribution significantly, especially for CH<sub>4</sub> hydrocarbon during APR and APH reaction. The reducibility of the supported platinum nanoparticles was also influenced by a surface acidity by altering a metal support interaction, and the strong interaction of the platinum nanoparticles with acid sites can be changed by shifting a reduction peak to a higher temperature and forming strong metal-support interaction on the strong acid sites of the solid-acid surfaces.<sup>43,68-74</sup> Based on the present observation, the surface acidity of the SiO<sub>2</sub>-Al<sub>2</sub>O<sub>3</sub> mixed metal oxides largely altered the dispersion of platinum nanoparticles with their interaction on the solid acid surfaces, which can also significantly altered EG conversion and hydrocarbon selectivity. In addition, the

selective coke deposition on the strong acid sites on the Pt/SA(0) also altered catalytic activity and product distribution, especially for hydrocarbon selectivity.

In summary, EG conversion and hydrocarbon distribution were strongly affected by the amount and type of acidic sites with the dispersion and reducibility of the supported platinum nanoparticles, which have a proper interaction with solid-acid  $\text{SiO}_2\text{-Al}_2\text{O}_3$  surfaces as shown in **Figure 7**. The stronger acid sites (or density of total acid sites) on the Pt/SA catalysts are preferentially responsible for a higher EG conversion through APR and APH reaction, i.e., EG conversion was increased with the increase of the strong acid sites through a first step of hydrogenolysis and dehydration of EG. However, the Pt/SA(0) having a too strong acid sites is responsible for a significant coke deposition by deactivating the Pt/SA(0) rapidly. In addition, a larger amount of weak Bronsted acid sites (or higher ratio of Bronsted/Lewis acid sites (B/L)), which seems to be interacted with the supported metallic platinum nanoparticles by forming a smaller platinum crystallite size of below 5 nm, is responsible for a higher  $\text{CH}_4$  hydrocarbon selectivity through a subsequent hydrogenation and WGS activity to form  $\text{CO}_2$  simultaneously during APR and APH reaction. Therefore, the proper controls of the amount and type of the acid sites by adjusting the metal-support interaction on the Pt/SA catalysts are important to enhance catalytic activity for a transformation of biomass-derived intermediates during APR and APH reaction, which can be simply obtained by changing Si/Al molar ratio on the Pt/SA catalysts.

#### 4. Conclusions

The platinum supported  $\text{SiO}_2\text{-Al}_2\text{O}_3$  catalysts were found to be efficient and simple catalytic system for a chemical transformation of biomass-derived intermediates to useful hydrogen and paraffinic hydrocarbons. A larger metallic surface area of the platinum nanoparticles with a proper interaction with Bronsted acid sites on the  $\text{SiO}_2\text{-Al}_2\text{O}_3$  support was responsible for

the large hydrocarbon selectivity through a hydrogenation and WGS reaction. In addition, the stronger Bronsted acid sites play an important role to enhance EG conversion to gaseous hydrogen product during APR and APH reaction. The APR and APH reaction proceeded through the consecutive reaction pathways, where the strong acid sites on the Pt/SA catalysts act as active sites for hydrogenolysis of C-C and C-O bond cleavages. The weak Bronsted acid sites are related with the dispersion of the supported platinum nanoparticles, which are also responsible for a higher reducibility and WGS activity as well. Even though the total acid sites with their types and the reducibility of platinum nanoparticles was well correlated with the catalytic activity of APR and APH, the catalyst deactivation on the Pt/SA(0) during APR reaction was strongly affected by the heavy coke deposition on the stronger acid sites. With an increase of Si/Al on the SiO<sub>2</sub>-Al<sub>2</sub>O<sub>3</sub> mixed metal oxides, EG conversion was decreased due to the decreased first step activity such as hydrogenolysis and dehydration of EG originated from the smaller amount of stronger acid sites, and Pt/SA(0.1) was found to be an optimal catalyst for APR and APH reaction, which can be easily prepared by simply changing Si/Al molar ratio of the Pt/SA catalysts.

### Acknowledgments

The present study was financially supported by the grant from the Industrial Source Technology Development Programs (2013-10042712) of the Ministry of Knowledge Economy (MKE) of Korea. The authors would like to acknowledge the financial support from the National Research Foundation of Korea (NRF) grant funded by the Korea government (NRF-2014R1A1A2A16055557 and NRF-2016M3D3A1A01913253). This work was supported by an institutional program Grant (2E26570-16-037) from Korean Institute of Science and Technology.

## References

1. J. C. Serrano-Ruiz and J. A. Dumesic, *Energy Environ. Sci.*, 2011, **4**, 83-99.
2. A. J. Ragauskas, C. K. Williams, B. H. Davison, G. Britovsek, J. Cairney, C. A. Eckert, W. J. Frederick, J. P. Hallett, D. J. Leak, C. L. Liotta, J. R. Mielenz, R. Murphy, R. Templer and T. Tschaplinski, *Science*, 2006, **311**, 484-489.
3. J. R. Rostrup-Nielsen, *Science*, 2005, **308**, 1421-1422.
4. R. R. Davda, J. W. Shabaker, G. W. Huber, R. D. Cortright and J. A. Dumesic, *Appl. Catal. B: Environ.*, 2003, **43**, 13-26.
5. R. R. Davda, J. W. Shabaker, G. W. Huber, R. D. Cortright and J. A. Dumesic, *Appl. Catal. B: Environ.*, 2005, **56**, 171-186.
6. J. W. Shabaker, G. W. Huber, R. R. Davda, R. D. Cortright and J. A. Dumesic, *Catal. Lett.*, 2003, **88**, 1-8.
7. J. W. Shabaker and J. A. Dumesic, *Ind. Eng. Chem. Res.*, 2004, **43**, 3105-3112.
8. C. H. Bartholomew, *Appl. Catal. A: Gen.*, 2001, **212**, 17-60.
9. C. H. Bartholomew, *Catal. Rev.*, 1982, **24**, 67-112.
10. D. J. M. de Vlieger, B. L. Mojet, L. Lefferts and K. Seshan, *J. Catal.*, 2012, **292**, 239-245.
46. A. Wawrzetz, B. Peng, A. Hrabar, A. Jentys, A. A. Lemonidou and J. A. Lercher, *J. Catal.*, 2010, **269**, 411-420.
11. X. Hu and G. Lu, *Appl. Catal. B: Environ.*, 2009, **88**, 376-385.
12. P. N. Kechagiopoulos, S. S. Voutetakis, A. A. Lemonidou and I. A. Vasalos, *Energy Fuels*, 2006, **20**, 2155-2163.
13. D. Mei, V. Lebarbier Dagle, R. Xing, K. O. Albrecht and R. A. Dagle, *ACS Catal.*, 2016, **6**, 315-325.
14. D. M. Alonso, S. G. Wettstein and J. A. Dumesic, *Chem. Soc. Rev.*, 2012, **41**, 8075-8098.
15. X.-K. Gu, B. Liu and J. Greeley, *ACS Catal.*, 2015, **5**, 2623-2631.

16. M. Saliccioli and D. G. Vlachos, *ACS Catal.*, 2011, **1**, 1246-1256.
17. S. Kandoi, J. Greeley, D. Simonetti, J. Shabaker, J. A. Dumesic and M. Mavrikakis, *J. Phys. Chem. C*, 2011, **115**, 961-971.
18. T. Nozawa, Y. Mizukoshi, A. Yoshida and S. Naito, *Appl. Catal. B: Environ.*, 2014, **146**, 221-226.
19. R. Rinaldi and F. Schuth, *Energy Environ. Sci.*, 2009, **2**, 610-626.
20. J. Lee, Y. Xu and G. W. Huber, *Appl. Catal. B: Environ.*, 2013, **140-141**, 98-107.
21. G. W. Huber, R. D. Cortright and J. A. Dumesic, *Angew. Chemie Int. Ed.*, 2004, **43**, 1549-1551.
22. P. Ferrin, D. Simonetti, S. Kandoi, E. Kunkes, J. A. Dumesic, J. K. Nørskov and M. Mavrikakis, *J. Am. Chem. Soc.*, 2009, **131**, 5809-5815.
23. B. M. Moreno, N. Li, J. Lee, G. W. Huber and M. T. Klein, *RSC Adv.*, 2013, **3**, 23769-23784.
24. N. Li and G. W. Huber, *J. Catal.*, 2010, **270**, 48-59.
25. M. Saliccioli, W. Yu, M. A. Barteau, J. G. Chen and D. G. Vlachos, *J. Am. Chem. Soc.*, 2011, **133**, 7996-8004.
26. K. L. Deutsch, D. G. Lahr and B. H. Shanks, *Green Chem.*, 2012, **14**, 1635-1642.
27. J. Greeley and M. Mavrikakis, *J. Am. Chem. Soc.*, 2004, **126**, 3910-3919.
28. J. Greeley and M. Mavrikakis, *J. Am. Chem. Soc.*, 2002, **124**, 7193-7201.
29. W. Luo and A. Asthagiri, *J. Phys. Chem. C*, 2014, **118**, 15274-15285.
30. S. Sa, H. Silva, L. Brandão, J. M. Sousa and A. Mendes, *Appl. Catal. B: Environ.*, 2010, **99**, 43-57.
31. J. Lee, Y. T. Kim and G. W. Huber, *Green Chem.*, 2014, **16**, 708-718.
32. J. Yang, C. L. Williams, A. Ramasubramaniam and P. J. Dauenhauer, *Green Chem.*, 2014, **16**, 675-682.

33. C. Zhang, J. Xing, L. Song, H. Xin, S. Lin, L. Xing and X. Li, *Catal. Today*, 2014, **234**, 145-152.
34. D. B. Lao, A. C. E. Owens, D. M. Heinekey and K. I. Goldberg, *ACS Catal.*, 2013, **3**, 2391-2396.
35. Y. Nakagawa and K. Tomishige, *Catal. Sci. Technol.*, 2011, **1**, 179-190.
36. Y. Amada, Y. Shinmi, S. Koso, T. Kubota, Y. Nakagawa and K. Tomishige, *Appl. Catal. B: Environ.*, 2011, **105**, 117-127.
37. Y. T. Kim, K.-D. Jung and E. D. Park, *Appl. Catal. B: Environ.*, 2011, **107**, 177-187.
38. R. Weingarten, G. A. Tompsett, W. C. Conner Jr. and G. W. Huber, *J. Catal.*, 2011, **279**, 174-182.
39. L. Yang, G. Tsilomelekis, S. Caratzoulas and D. G. Vlachos, *ChemSusChem*, 2015, **8**, 1334-1341.
40. K. Okada, T. Tomita, Y. Kameshima, A. Yasumori and K. J. D. MacKenzie, *J. Mater. Chem.*, 1999, **9**, 1307-1312.
41. S. Jeon, H. W. Ham, Y. W. Suh and J. W. Bae, *RSC Adv.*, 2015, **5**, 54806-54815.
42. A. Ciftci, B. Peng, A. Jentys, J. A. Lercher and E. J. M. Hensen, *Appl. Catal. A: Gen.*, 2012, **431-432**, 113-119.
43. A. Ciftci, D. A. J. M. Ligthart and E. J. M. Hensen, *Appl. Catal. B: Environ.*, 2015, **174-175**, 126-135.
44. K. Lehnert and P. Claus, *Catal. Commun.*, 2008, **9**, 2543-2546.
45. J. W. Bae, I. G. Kim, J. S. Lee, K. H. Lee and E. J. Jang, *Appl. Catal. A: Gen.*, 2003, **240**, 129-142.
46. M. Besson and P. Gallezot, *Catal. Today*, 2003, **81**, 547-559.
47. A. Ciftci, D. A. J. M. Ligthart, A. O. Sen, A. J. F. van Hoof, H. Friedrich and E. J. M. Hensen, *J. Catal.*, 2014, **311**, 88-101.

48. A. Ciftci, D. A. J. M. Ligthart and E. J. M. Hensen, *Green Chem.*, 2014, **16**, 853-863.
49. B. Sanchez, M. S. Gross, B. D. Costa and C. A. Querini, *Appl. Catal. A: Gen.*, 2009, **364**, 35-41.
50. A. Iriondo, J. F. Cambra, V. L. Barrio, M. B. Guemez, P. L. Arias, M. C. Sanchez-Sanchez, R. M. Navarro and J. L. G. Fierro, *Appl. Catal. B: Environ.*, 2011, **106**, 83-93.
51. Z. Zhong, H. Ang, C. Choong, L. Chen, L. Huang and J. Lin, *Phys. Chem. Chem. Phys.*, 2009, **11**, 872-880.
52. M. Niwa, K. Awano and Y. Murakami, *Appl. Catal.*, 1983, **7**, 317-325.
53. U. Nylén, J. F. Delgado, S. Järås and M. Boutonnet, *Appl. Catal. A: Gen.*, 2004, **262**, 189-200.
54. J. H. Park, C. Pang, C. H. Chung and J. W. Bae, *J. Nanosci. Nanotechnol.*, 2016, **16(5)**, 4626-4630.
55. S. Y. Park, C. H. Shin and J. W. Bae, *Catal. Commun.*, 2016, **75**, 28-31.
56. J. W. Jung, Y. J. Lee, S. H. Um, P. J. Yoo, D. H. Lee, K. W. Jun and J. W. Bae, *Appl. Catal. B: Environ.*, 2012, **126**, 1-8.
58. G. S. Foo, D. Wei, D. S. Sholl and C. Sievers, *ACS Catal.*, 2014, **4**, 3180-3192.
59. G. Yaluris, R. B. Larson, J. M. Kobe, M. R. González, K. B. Fogash and J. A. Dumesic, *J. Catal.*, 1996, **158**, 336-342.
60. C. D. Baertsch, K. T. Komala, Y.-H. Chua and E. Iglesia, *J. Catal.*, 2002, **205**, 44-57.
61. M. Watanabe, Y. Aizawa, T. Iida, R. Nishimura and H. Inomata, *Appl. Catal. A: Gen.*, 2005, **295**, 150-156.
62. V. V Ordonsky and A. Y. Khodakov, *Green Chem.*, 2014, **16**, 2128-2131.
63. Y. T. Kim, J. A. Dumesic and G. W. Huber, *J. Catal.*, 2013, **304**, 72-85.
64. K. Nakajima, Y. Baba, R. Noma, M. Kitano, J. N. Kondo, S. Hayashi and M. Hara, *J. Am. Chem. Soc.*, 2011, **133**, 4224-4227.

65. S. Rajagopal, J. A. Marzari and R. Miranda, *J. Catal.*, 1995, **151**, 192-203.
66. L. Wang, H. Wan, S. Jin, X. Chen, C. Li and C. Liang, *Catal. Sci. Technol.*, 2015, **5**, 465-474.
67. D. G. Rethwisch and J. A. Dumesic, *Langmuir*, 1986, **2**, 73-79.
68. C. W. Chou, S. J. Chu, H. J. Chiang, C. Y. Huang, C. Lee, S. R. Sheen, T. P. Perng and C. Yeh, *J. Phys. Chem. B*, 2001, **105**, 9113-9117.
69. P. Panagiotopoulou, A. Christodoulakis, D. I. Kondarides and S. Boghosian, *J. Catal.*, 2006, **240**, 114-125.
70. A. S. Ivanova, E. M. Slavinskaya, R. V Gulyaev, V. I. Zaikovskii, O. A. Stonkus, I. G. Danilova, L. M. Plyasova, I. A. Polukhina and A. I. Boronin, *Appl. Catal. B: Environ.*, 2010, **97**, 57-71.
71. J. N. Kuhn, W. Huang, C. K. Tsung, Y. Zhang and G. A. Somorjai, *J. Am. Chem. Soc.*, 2008, **130**, 14026-14027.
72. Q. Liu, U. A. Joshi, K. Uber and J. R. Regalbuto, *Phys. Chem. Chem. Phys.*, 2014, **16**, 26431-26435.
73. C. Serre, F. Garin, G. Belot and G. Maire, *J. Catal.*, 1993, **141**, 1-8.
74. G. Jacobs, U. M. Graham, E. Chenu, P. M. Patterson, A. Dozier and B. H. Davis, *J. Catal.*, 2005, **229**, 499-512.

**Figure captions**

**Figure 1.** Conversion of EG to gaseous products with time on stream on the Pt/SA catalysts for APR reaction at the reaction conditions of  $T = 250\text{ }^{\circ}\text{C}$ ,  $P = 4.5\text{ MPa}$  and weight hourly space velocity (WHSV) =  $2.0\text{ h}^{-1}$  with 0.3 g catalyst using 10wt%EG in an aqueous solution

**Figure 2.** Conversion of EG to gaseous products with time on stream on the Pt/SA catalysts for APH reaction at the reaction conditions of  $T = 260\text{ }^{\circ}\text{C}$ ,  $P = 5.0\text{ MPa}$  and weight hourly space velocity (WHSV) =  $0.6\text{ h}^{-1}$  with 0.5 g catalyst using 10wt%EG in an aqueous solution

**Figure 3.** XRD patterns of the Pt/SA catalysts after APR reaction for 20 h

**Figure 4.**  $\text{H}_2$ -TPR profiles of the fresh Pt/SA catalysts

**Figure 5.**  $\text{NH}_3$ -TPD profiles on the fresh Pt/SA catalysts

**Figure 6.** TEM images on the selected Pt/SA catalysts; (A-1) fresh Pt/SA(0), (A-2) used Pt/SA(0), (B-1) fresh Pt/SA(0.1) and (B-2) used Pt/SA(0.1)

**Figure 7.** Conversion of EG to gaseous products and hydrocarbon (HC) selectivity for APR and APH reaction as well as the density of total acid sites and the ratio of Bronsted/Lewis acid sites in terms of the Si/Al molar ratios on the Pt/SA catalysts

**Table 1.** Aqueous phase reforming (APR)<sup>a</sup> and aqueous phase hydrodeoxygenation (APH)<sup>b</sup> reaction over the Pt/SA catalysts

Notation	Aqueous phase reforming (APR)							Aqueous phase hydrodeoxygenation (APH)							
	Conversion to gases (%) / production rate of H <sub>2</sub> (mL/(g <sub>cat</sub> h))	Selectivity of products (mol%)				Selectivity of hydrocarbons (mol%)			Conversion to gases (%) / production rate of HC <sup>c</sup> (mL/(g <sub>cat</sub> h))	Selectivity of products (mol%)			Selectivity of hydrocarbons (mol%)		
		H <sub>2</sub>	CO	CO <sub>2</sub>	HC <sup>c</sup>	CH <sub>4</sub>	C <sub>2</sub>	CO		CO <sub>2</sub>	HC <sup>c</sup>	CH <sub>4</sub>	C <sub>2</sub>	C <sub>3</sub>	
Pt/SA(0)	27.5 / 1076	73.1	0.4	25.3	1.2	20.5	79.5	42.7 / 1.4	1.1	96.2	2.7	46.0	50.9	3.1	
Pt/SA(0.1)	43.4 / 1691	72.9	0.8	25.4	0.9	36.2	63.8	47.9 / 2.0	2.6	93.8	3.6	52.7	47.3	0.0	
Pt/SA(0.4)	30.7 / 1178	72.7	1.8	23.9	1.6	57.7	42.3	46.8 / 4.0	2.0	90.9	7.1	53.1	45.9	1.0	
Pt/SA(1.0)	18.4 / 657	71.3	5.2	21.0	2.5	64.5	35.5	29.0 / 3.1	14.7	76.3	9.0	56.1	42.8	1.1	
Pt/SA(0.1) <sup>d</sup>	64.6 / 1251	72.8	0.3	25.5	1.4	47.9	52.1	-	-	-	-	-	-	-	
Pt/SA(0.1) <sup>e</sup>	78.6 / 730	72.0	1.5	24.5	2.0	78.1	21.9	-	-	-	-	-	-	-	

<sup>a</sup>APR reaction was carried out in a fixed-bed tubular reactor at the reaction conditions of T = 250 °C, P = 4.5 MPa and weight hourly space velocity (WHSV) = 2.0 h<sup>-1</sup> with 0.3 g catalyst using 10wt% ethylene glycol (EG) in an aqueous solution. The conversion and selectivity are the averaged values at steady-state after the reaction of 15 h on stream.

<sup>b</sup>APH reaction was carried out in a fixed-bed tubular reactor at the reaction conditions of T = 260 °C, P = 5.0 MPa and weight hourly space velocity (WHSV) = 0.6 h<sup>-1</sup> with 0.5 g catalyst using 10wt% ethylene glycol (EG) in an aqueous solution. The conversion and selectivity are the averaged values at steady-state after the reaction of 15 h on stream.

<sup>c</sup>HC stands for the hydrocarbons formed during APR and APH reaction, which are mainly paraffinic hydrocarbons such as methane (CH<sub>4</sub>), ethane (C<sub>2</sub>) and propane (C<sub>3</sub>).

<sup>d,e</sup>APR reaction was carried out in a fixed-bed tubular reactor at the reaction conditions of T = 250 °C, P = 4.5 MPa and weight hourly space velocity (WHSV) = 1.0 h<sup>-1</sup> (d) and 0.5 h<sup>-1</sup> (e) with 0.3 g catalyst using 10wt% ethylene glycol (EG) in an aqueous solution, respectively.

**Table 2.** Physicochemical properties of the Pt/SA catalysts before and after APR reaction

Notation	XRF (Si/Al molar ratio)	N <sub>2</sub> sorption <sup>a</sup>			H <sub>2</sub> chemisorption <sup>b</sup>			TPR <sup>c</sup> ( $\mu\text{molH}_2/\text{g}_{\text{cat}}$ )			NH <sub>3</sub> -TPD <sup>d</sup> ( $\text{mmolNH}_3/\text{g}_{\text{cat}}$ )			Py- IR <sup>e</sup> B/L	Coke (%) from TGA	
		Sg ( $\text{m}^2/\text{g}$ )	Pv ( $\text{cm}^3/\text{g}$ )	Ps (nm)	Sg(sup) ( $\text{m}^2/\text{g}$ )	D (%)	Sg ( $\text{m}^2/\text{g}$ )	Dp (nm)	T <sub>L</sub>	T <sub>M</sub>	T <sub>H</sub>	T <sub>w</sub>	T <sub>s</sub>			T <sub>tot</sub>
Pt/SA(0)	0	302	0.24	3.1	370	45.7	5.64	2.54	157	104	72	0.45	5.94	6.39	0	10.0
Pt/SA(0.1)	0.12	321	0.46	4.6	415	61.9	7.65	1.86	52	87	-	0.58	5.18	5.76	0.61	3.9
Pt/SA(0.4)	0.46	338	0.53	5.2	462	63.9	7.89	1.81	38	181	-	0.77	4.22	4.99	0.95	5.0
Pt/SA(1.0)	0.89	384	0.55	4.6	496	63.5	7.85	1.82	23	188	-	0.75	3.80	4.55	1.22	5.9

<sup>a</sup>Sg, Pv, and Ps measured by N<sub>2</sub> adsorption-desorption analysis represent the surface area ( $\text{m}^2/\text{g}$ ), pore volume( $\text{cm}^3/\text{g}$ ) and average pore diameter (nm) of the Pt/SA catalysts, respectively. The Sg(sup) represents the surface area ( $\text{m}^2/\text{g}$ ) of the SA support itself.

<sup>b</sup>D, Sg and Dp measured by H<sub>2</sub> chemisorption represent the dispersion (%), surface area ( $\text{m}^2/\text{g}$ ) and average crystallite size (nm) of metallic platinum on the Pt/SA catalysts, respectively.

<sup>c</sup>The amount of consumed hydrogen from TPR was denoted as T<sub>L</sub>, T<sub>M</sub> and T<sub>H</sub> for the consumed amount of hydrogen in the temperature range of < 200, 200 - 500, and >500 °C, respectively with a unit of  $\mu\text{molH}_2/\text{g}_{\text{cat}}$ .

<sup>d</sup>The amount of acid sites measured by NH<sub>3</sub>-TPD with a unit of  $\text{mmolNH}_3/\text{g}_{\text{cat}}$  was denoted as T<sub>w</sub>, T<sub>s</sub> and T<sub>tot</sub> for weak, strong acid sites with total amount of acid sites in the temperature range of < 300 and 300 - 500 °C, respectively.

<sup>e</sup>The characteristic absorption peaks of pyridine molecules were assigned to Bronsted acidic site (B) at a wave number of 1550  $\text{cm}^{-1}$  and Lewis acidic site (L) at that of 1450  $\text{cm}^{-1}$ , and the ratio of B/L on the Pt/SA catalysts was calculated using those relative integrated areas.

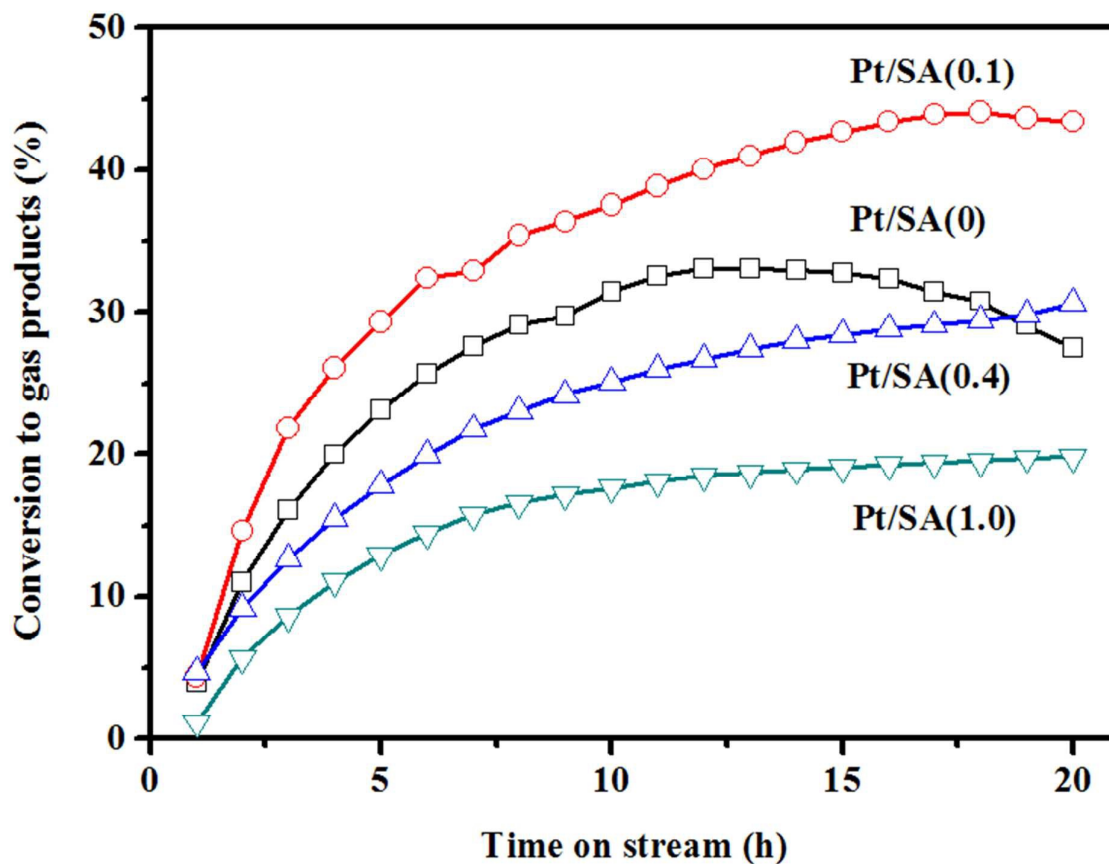


**Figure 1.** Conversion of EG to gaseous products with time on stream on the Pt/SA catalysts for APR reaction at the reaction conditions of  $T = 250\text{ }^{\circ}\text{C}$ ,  $P = 4.5\text{ MPa}$  and weight hourly space velocity (WHSV) =  $2.0\text{ h}^{-1}$  with 0.3 g catalyst using 10wt%EG in an aqueous solution

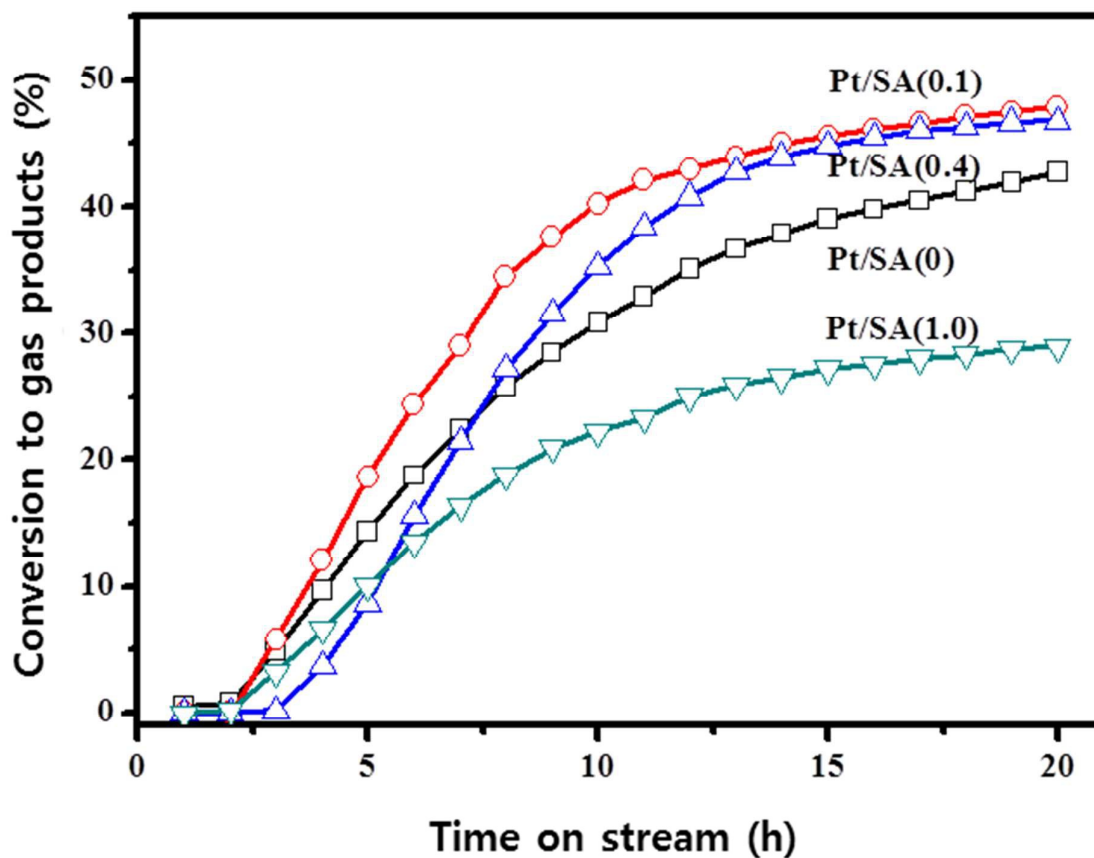


**Figure 2.** Conversion of EG to gaseous products with time on stream on the Pt/SA catalysts for APH reaction at the reaction conditions of  $T = 260\text{ }^{\circ}\text{C}$ ,  $P = 5.0\text{ MPa}$  and weight hourly space velocity (WHSV) =  $0.6\text{ h}^{-1}$  with 0.5 g catalyst using 10wt%EG in an aqueous solution

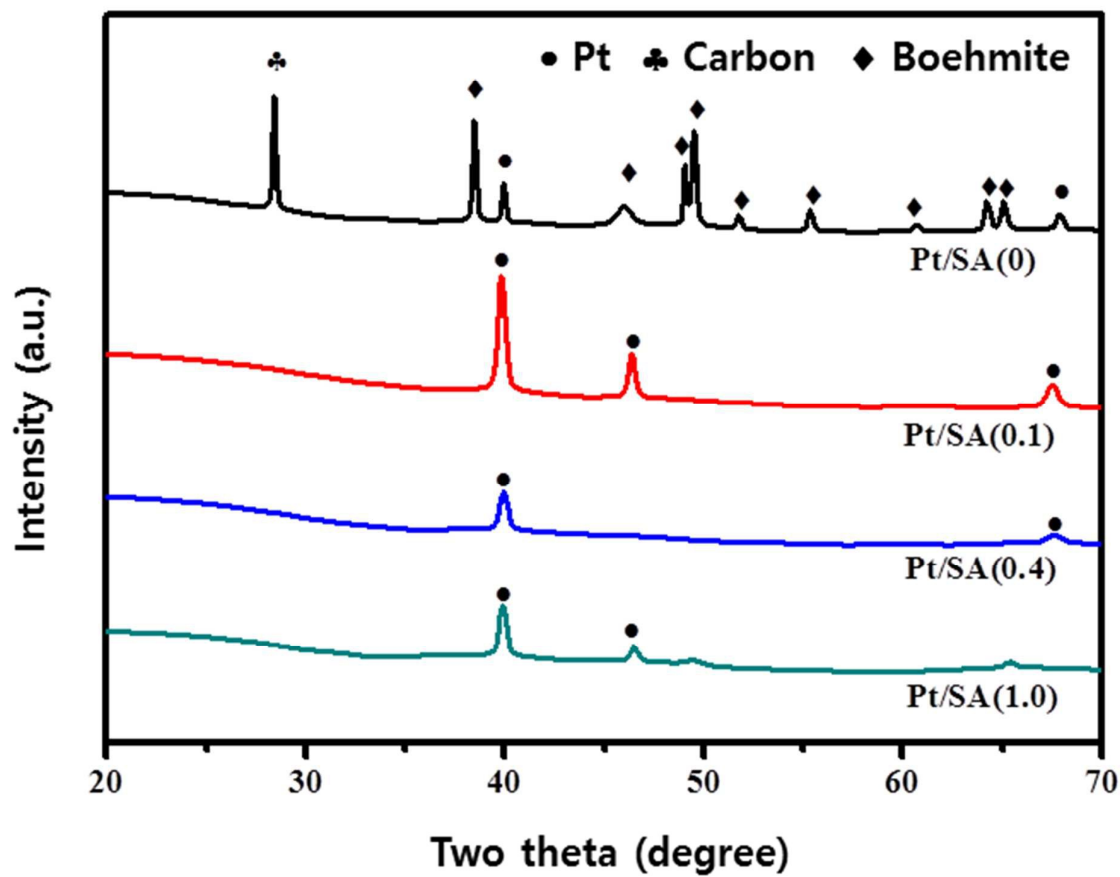


**Figure 3.** XRD patterns of the used Pt/SA catalysts after APR reaction for 20 h

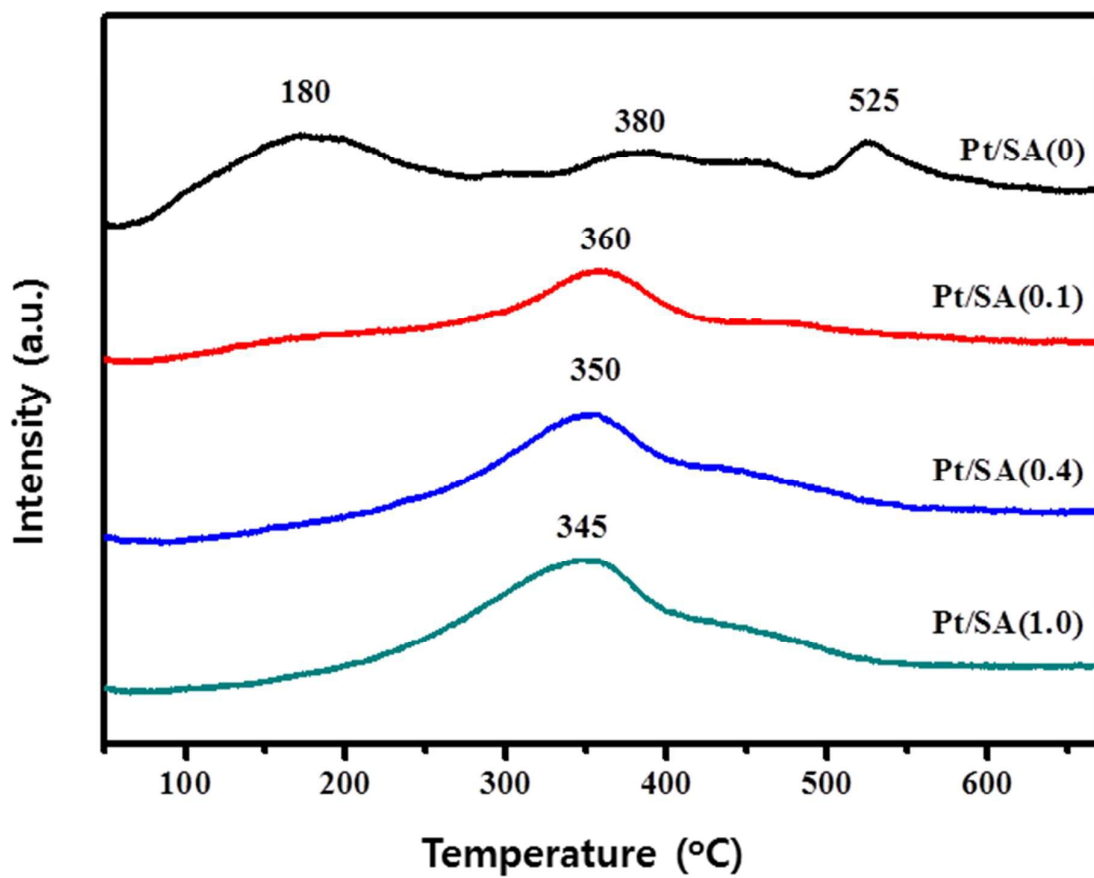


**Figure 4.** H<sub>2</sub>-TPR profiles of the fresh Pt/SA catalysts

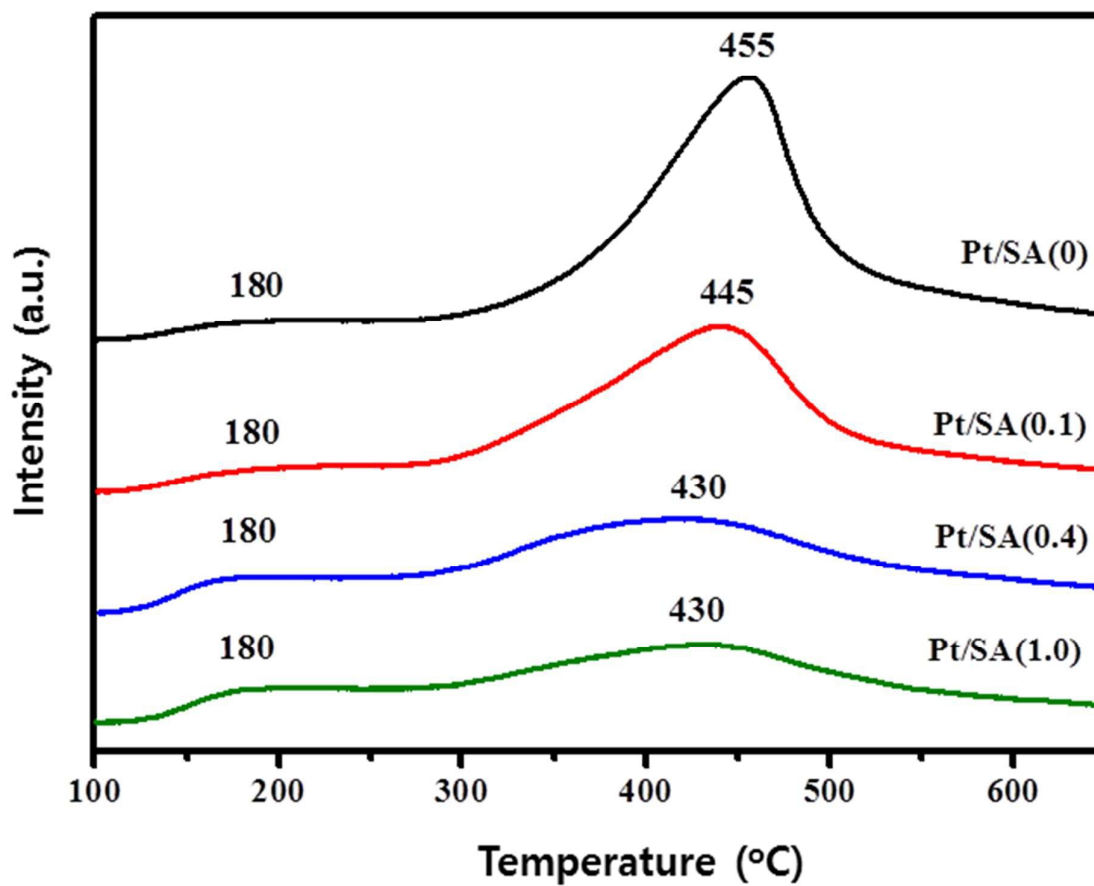
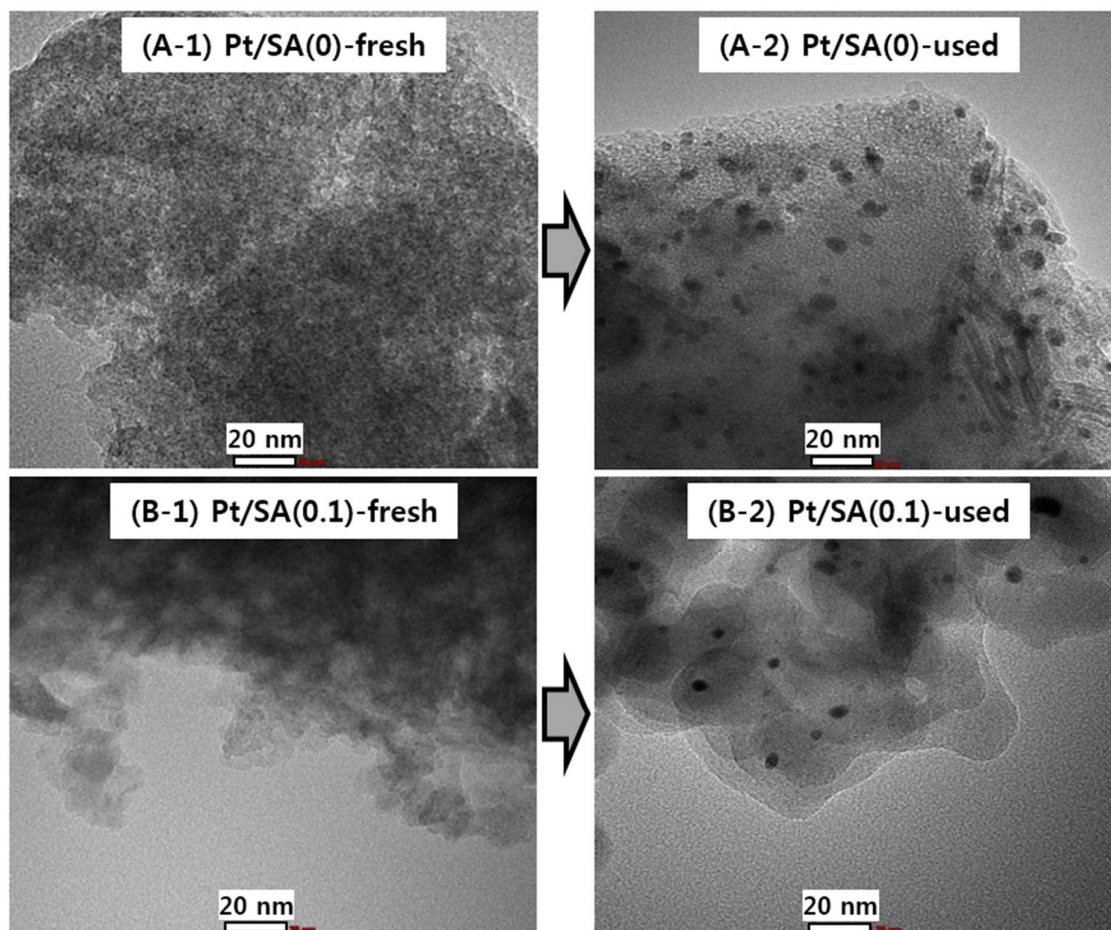
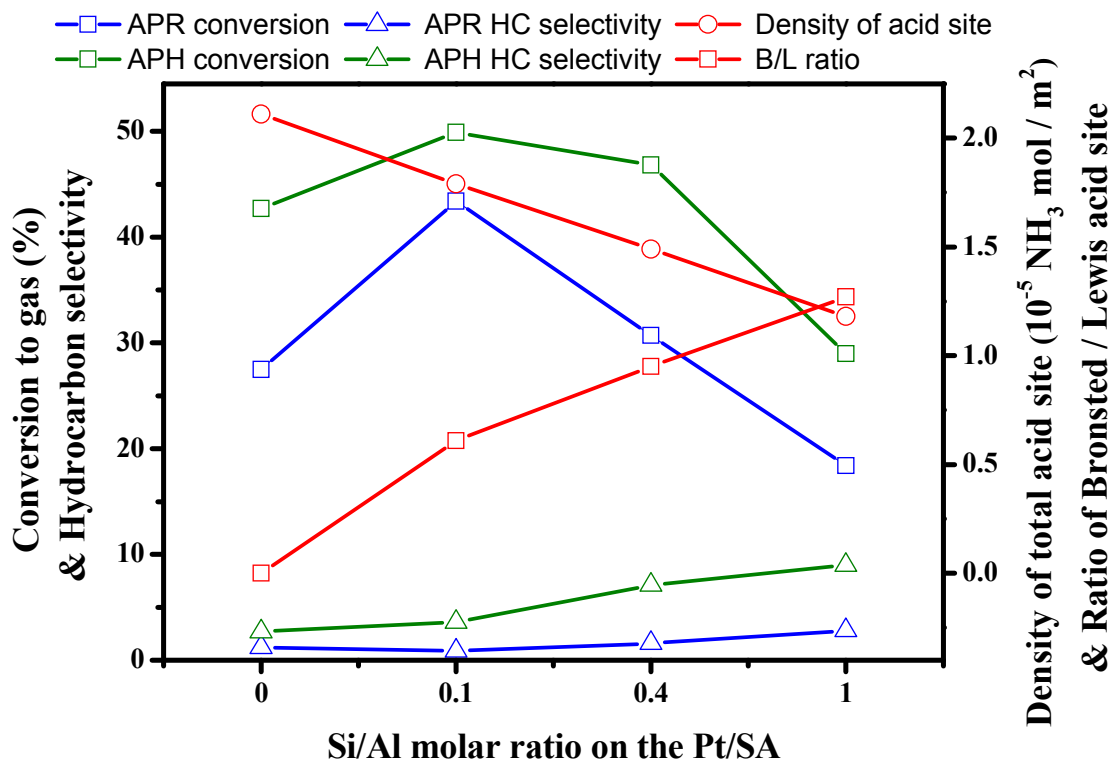


Figure 5.  $\text{NH}_3$ -TPD profiles on the fresh Pt/SA catalysts



**Figure 6.** TEM images on the selected Pt/SA catalysts; (A-1) fresh Pt/SA(0), (A-2) used Pt/SA(0), (B-1) fresh Pt/SA(0.1) and (B-2) used Pt/SA(0.1)



**Figure 7.** Conversion of EG to gaseous products and hydrocarbon (HC) selectivity for APR and APH reaction as well as the density of total acid sites and the ratio of Bronsted/Lewis acid sites in terms of the Si/Al molar ratios on the Pt/SA catalysts

Aqueous-phase reforming (APR) and aqueous-phase hydrodeoxygenation (APH) reaction of ethylene glycol (EG) were investigated on the Pt/SiO<sub>2</sub>-Al<sub>2</sub>O<sub>3</sub>, and the Pt/SA(0.1) having a Si/Al ratio of 0.1 showed a higher catalytic activity due to the presence of larger amount of acidic sites with a smaller platinum crystallite and a lower coke deposition.

